Non-Ionic Fluorosurfactants for Droplet-Based *in vivo* Applications

Heidi L. van de Wouw,[a] Shuo-Ting Yen,[b,c] Manon Valet,[b] Joseph Garcia,[a] Antoine Vian,[b,c] Yucen Liu,[c] Jennifer Pollock,[c] Otger Campàs*[b,c,d] and Ellen M. Sletten*[a]

[a] Dr. Heidi L. van de Wouw; Joseph Garcia; Dr. Ellen M. Sletten
Department of Chemistry and Biochemistry
University of California, Los Angeles
607 Charles E. Young Drive E., Los Angeles, CA 90095, USA

[b] Dr. Shuo-Ting Yen; Dr. Manon Valet; Dr. Antoine Vian; Dr. Otger Campàs
Cluster of Excellence Physics of Life
TU Dresden
Arnoldstrasse 18, 01307 Dresden, Germany

[c] Dr. Shuo-Ting Yen; Dr. Antoine Vian, Yucen Liu; Jennifer Pollock; Dr. Otger Campàs
Department of Mechanical Engineering
University of California, Santa Barbara
Santa Barbara, CA 93106, USA

[d] Dr. Otger Campàs
Max Planck Institute of Molecular Cell Biology and Genetics
Center for Systems Biology Dresden
Pfotenhauerstrasse 108, 01307 Dresden, Germany

Abstract: Fluorocarbon oils are uniquely suited for many biomedical applications due to their inert, bioorthogonal properties. In order to interface fluorocarbon oils with biological systems, non-ionic fluorosurfactants are necessary. However, there is a paucity of non-ionic fluorosurfactants with low interfacial tension to stabilize fluorocarbon phases in aqueous environments (such as oil-in-water emulsions). We developed non-ionic fluorosurfactants composed of a polyethylene glycol (PEG) segment covalently bonded to a flexible perfluoropolyether (PFPE) segment that confer lower interfacial tensions (IFTs) between a fluorocarbon oil, HFE-7700, and water. Synthesis of a panel of surfactants spanning a molecular weight range of 0.64–66 kDa with various hydrophilic-lipophilic balances allowed for identification of minimal IFTs, ranging from 1.4 to 17.8 mN m^{-1}. The majority of these custom fluorosurfactants display poor solubility in water, allowing their co-introduction with fluorocarbon oils and minimal leaching. We applied the PEG$_5$PFPE$_1$ surfactant for mechanical force measurements in zebrafish, enabling exceptional sensitivity.

Introduction

Perfluorocarbons form an inert "fluorous phase" that is orthogonal to aqueous and organic solutions. The abiotic nature of the fluorous phase provides unique opportunities to engineer sensors,[1] delivery agents,[2] and microcompartments[3] that do not interfere with living systems. From the chemical perspective, a critical component of all these fluorous technologies is the ability to control the interface between the perfluorocarbon and water phases, while retaining orthogonality to biological systems.[4,5]

Interfaces between two immiscible phases are stabilized by surfactants. The efficiency of the surfactant can be quantified by the interfacial tension (IFT) between the phases.[6] While considerable efforts have been directed toward elucidating structure-property relationships for the stabilization of water/organic interfaces,[7] the selection of surfactants to stabilize the water/perfluorocarbon interface is limited. Efforts toward fluorosurfactant development surround two main areas: 1) the stabilization of perfluorocarbon-in-water droplets for emulsion polymerizations[8] and 2) the stabilization of water-in-perfluorocarbon droplets[9–13] for microfluidics. Surfactants toward the former have primarily contained an anionic carboxylate appended to a short (C_6–C_{10}) perfluoroalkyl moiety. While their ability to stabilize perfluorocarbon/water interfaces is excellent, with interfacial tensions as low as 15-20 mN m^{-1},[14] they are "PFAS" which display significant bioaccumulation concerns.[15,16] Furthermore, their ionic nature promotes interactions with biomolecules and changes in pH or ionic strength can considerably alter the IFT.[14,17] Thus, these ionic fluorosurfactants are not optimal for use in biological applications.

Conversely, fluorosurfactants developed for microfluidics are considerably more biocompatible as they are commonly used to form droplets which contain living cells.[4,5,18,19] These surfactants are often composed of a hydrophilic poly(ethylene glycol) (PEG), which displays minimal protein adsorption, and a fluorous perfluoropolyether (PFPE) (Figure 1a). One of the most successful custom surfactants for water-in-perfluorocarbon microfluidics is the triblock copolymer **KP600** consisting of a short PEG segment (*n* = 13) flanked by two longer PFPE segments (*m* = 41) (Figure 1b,c).[4] More recent work exploring a series of diblock surfactants has also yielded low IFT water-in-perfluorocarbon droplets.[6]

We aimed to retain the biocompatibility of fluorosurfactants established for water-in-perfluorocarbon microfluidics,[20,21] yet optimize them for stabilizing perfluorocarbon-in-water droplets, which are more relevant to *in vivo* applications. Perfluorocarbon-in-water droplets have seen utility as blood substitutes,[22] biomolecule delivery vehicles,[23–25] multifunctional materials for photodynamic therapy,[26] and ultrasound contrast agents,[27–30] among others. Moreover, cell-sized perfluorocarbon-in-water droplets are essential for *in vivo* measurements of intercellular forces,[31,32] tissue material properties,[33,34] and osmotic pressures.[1] These latter applications require low IFT droplets, ideally less than 2 mN m^{-1}, and that the IFT does not change in response to the surrounding biological environment. Additional considerations for fluorosurfactant development for *in vivo* applications include preferential fluorous solubility over aqueous and organic mixtures, which

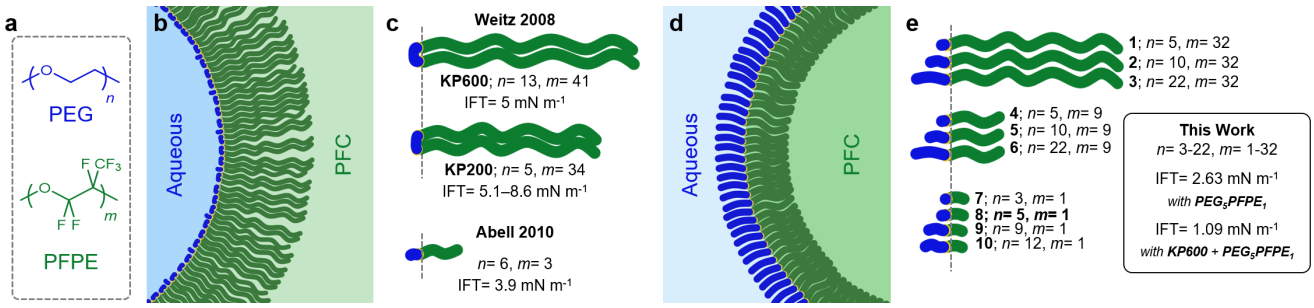

Figure 1. Non-ionic fluorosurfactants composed of a) water soluble polyethylene glycol (PEG, *n* repeats) and perfluorocarbon (PFC) soluble perfluoropolyether (PFPE, *m* repeats) segments for stabilization of b) water-in-PFC droplets with c) previously reported triblock copolymer surfactants, including commercially available **KP600** and a diblock copolymer surfactant (*n* = 6, *m* = 3) that provides a low interfacial tension (IFT) benchmark. d) PFC-in-water microdroplets stabilized by e) diblock copolymer surfactants **1**–**10** (*n* = 3-22, *m* = 1-32) synthesized and reported herein to optimize low IFT and high PFC solubility for PFC-in-water microdroplets. Surfactant **8**, or **PEG$_5$PFPE$_1$**, (*n* = 5, *m* = 1) surpassed previous low IFT benchmarks with an IFT= 2.88 mN m^{-1} and a mixed surfactant system of **KP600** + **PEG$_5$PFPE$_1$** produced a minimal IFT= 1.09 mN m^{-1}.

minimizes leakage of the fluorosurfactant to the surrounding environment while also facilitating co-introduction of the surfactant and perfluorocarbon.

Here we report a series of non-ionic PEG_n-$PFPE_m$ surfactants to stabilize perfluorocarbon-in-water droplets. We synthesize a series of surfactants and characterize their IFT for water/perfluorocarbon interfaces with HFE-7700 (structure in Figure S1) as the perfluorocarbon oil. We correlated IFT to the hydrophilic lipophilic balance of the surfactants. Then we select the **PEG_5PFPE_1** surfactant which has optimal solubility and IFT properties for *in vivo* measurements of mechanical forces, and measure cellular and tissue scale mechanical stresses within developing zebrafish embryos. Ultimately, we find that a mixture of the custom diblock fluorosurfactant **PEG_5PFPE_1** and **KP600** provides the most sensitive *in vivo* force measurements reported to date, enabling previously unattainable measurements.

Results and Discussion

Fluorosurfactant design and synthesis

To stabilize perfluorocarbon-in-water droplets, we focused on a diblock copolymer scaffold. The diblock copolymer geometry enables efficient packing of the surfactant molecule at the droplet surface (Figure 1d) without the need for bending the central hydrophilic group, as seen with **KP600** (Figure 1b). Based on the success of PEG and PFPE as hydrophilic and fluorous components of **KP600,** we chose these functionalities for the diblock surfactant panel. Specifically, we envisioned the flexibility of the PFPE segment (as compared to rigid perfluoroalkyls) would help with fluorous solubility, while the PEG would provide hydrophilicity without imparting ionic character. The PFPE lengths were dictated by commercial availability and the PEG lengths were then chosen to access a range of surfactants with varied hydrophilic–lipophilic balances (HLB). An amide bond was chosen for the linkage due to its small size, stability in biological environments, and straightforward synthesis. The PEG-amine reagents all contained a methoxy cap to prevent any esterification that would lead to the formation of triblock copolymers.

We synthesized a panel of 10 non-ionic, PEG_nPFPE_m diblock copolymer surfactants (**1**–**10**, Scheme 1). PFPE carboxylic acids (**$PFPE_m$-COOH**, m = 32, 9, 1) were activated as an acid chloride (**11**–**13**) and combined with an amino terminated PEG segment (**methoxyPEG_n-amine**, n = 3, 5, 10, 22). Quantitative conversion to the acid chloride and subsequent reaction with **methoxyPEG_n-amine** was essential as remaining **$PFPE_m$-COOH** was difficult to remove (with exception to m = 1) and displayed substantial surface activity which prevented accurate IFT measurements. Surfactants **1**–**6** were synthesized with a molar excess of anhydrous PEG to ensure quantitative coupling of **11** or **12** and facile removal of the water-soluble PEG starting material *via* dialysis (42-90% isolated yields). Surfactants **7**–**10** were synthesized with a molar excess of PFPE acid chloride **13**, as **$PFPE_1$-COOH** is volatile and could easily be removed with reduced pressure. Compounds **7** and **8** were isolated in 86% and 77% yield, respectively, while compounds **9** and **10** had reduced isolated yields (≤ 55%, using NMR determined values of n) as the starting **methoxy-PEG_{10}-amine** was disperse and the final products were resolved from the same starting reaction *via* silica gel column chromatography. To ensure formation of the amphiphilic surfactant and purification from parent PFPE acid, surfactants **1**–**10** were characterized by ATR-IR to confirm changes in the carbonyl stretch (Figure S2). ATR-IR analysis was further validated by ^{1}H- and ^{19}F-NMR end-group comparison using trifluorotoluene ($PhCF_3$) as an internal standard (Figure S3).

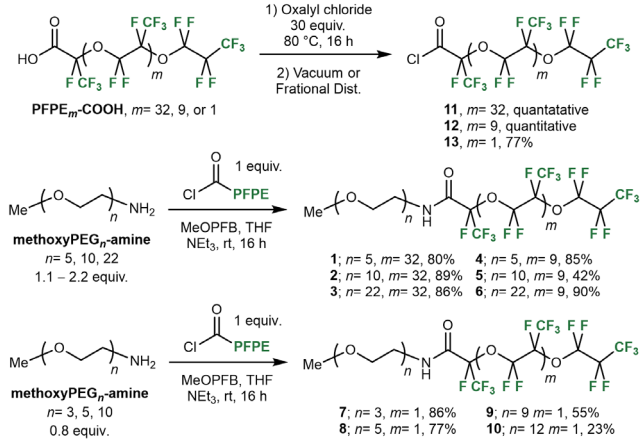

Scheme 1. Synthesis of amphiphile surfactants **1**–**10**. Activation of commercially available **$PFPE_m$-COOH** to acid chlorides **11**–**13** followed by reaction with commercially available **methoxyPEG_n-amine** to form surfactants **1**–**10**.

Surfactant solubility and stability

The overall water solubility of surfactants **1**–**10** was assessed by ^{19}F NMR (Figure S4). Neat surfactants **1**–**10** were vortexed against Milli-Q water for 5 min then rocked at room temperature for 24 h. An aliquot was lyophilized and redissolved in 5:2 C_6F_6/C_6D_6 with a $PhCF_3$ internal standard for quantification. Surfactants **1**–**5**, **7**, and **8** were not detected. Surfactants **6**, **9**, and **10** were determined to have solubilities of 4.1, 24, and 19 mM in water, respectively (Figure S4). For end use in biological applications, absence of water solubility is requisite for preventing the partition of the surface stabilizing surfactants into the aqueous matrix; therefore, surfactants **1**–**5**, **7**, and **8** have promising hydrophobic character.

A potential chemical liability of the surfactants is hydrolysis of the amide bond joining the amphiphilic segments. Hydrolysis of surfactants **1–10** would convert the non-ionic surfactant fluorosurfactant into an ionic PFPE-carboxylate, which would be detrimental to *in vivo* applications that require stable interfacial properties and long incubation times. The stability of the amide bond upon exposure to water was assessed over 6 d using liquid chromatography mass spectroscopic (LCMS) analysis. Representative surfactant **8** was incubated in 5% MeCN in water at 37 °C and analyzed at 0, 1.5, 2.5, and 6.0 d (Figure S5). No evidence of hydrolysis was observed by mass extraction analysis for both hydrolysis products, **methoxyPEG_5-amine** and **$PFPE_1$-COOH**, suggesting the amide bond is sufficiently stable within aqueous environments.

Measurement of surfactant IFTs at HFE-7700/water interface

Next, we investigated the ability for surfactants **1–10** to stabilize perfluorocarbon/water interfaces by assessing their ability to reduce the IFT. IFTs were measured by pendant droplet tensiometry where a droplet of perfluorocarbon oil containing the fluorous surfactant was suspended within water, the continuous phase (Figure S6a). Solutions of surfactants **1**–**10** at various concentrations were measured by pendant or spinning droplet tensiometry and values were recorded after an equilibrium was reached, the equilibrium IFT ($IFT_{equ.}$; Table S1). In general, as the concentration of surfactant increases, the measured IFT decreases to a minimal IFT value once the cmc is reached. IFTs measured from solutions with surfactant concentrations above the cmc were used to compare custom surfactants **1**–**10** (Table 1) against commercially available triblock copolymer surfactant **KP600** ($PFPE_m$-PEG_n-$PFPE_m$, m = 32, n = 13; $IFT_{equ.}$= 5.4 ± 0.4 mN m^{-1} at 3 mM, 2 wt%).

Surfactants **1**–**3** all consisted of a fluorous PFPE group with

Table 1. Measured interfacial tensions (IFTs) of fluorous surfactants **1**–**8** using pendant droplet tensiometry and **8**–**10** using spinning droplet tensiometry. Unless otherwise specified, all measurements were taken in triplicate using a droplet of perfluorocarbon solvent with surfactant pre-dissolved at the stated concentration and dispensed into bulk water. Reported IFTs are at concentrations above the cmc for each surfactant, as the average and standard deviation from multiple droplets. Additional data is available in Table S1.

Surfactant (n, m)[a]	HLB [b]	Concentration (mM)	Concentration (wt%)	IFT_{equ} (mN m^{-1})
1 (5, 32)	0.95	52	14%	14 ± 0.1
2 (10, 32)	1.6	26	8%	3.57 ± 0.03
3 (22, 32)	3.1	2.6	1%	17.8 ± 0.7[c]
4 (5, 9)	2.7	35	4%	14.3 ± 0.5
5 (10, 9)	4.4	1.3	0.2%	14.63 ± 0.03[c]
6 (22, 9)	7.3	0.26	0.04%	9 ± 1
7 (3, 1)	5.9	470	14%	11.33 ± 0.09
8 (5, 1)	7.6	336	12%	2.63 ± 0.08
8 (5, 1)[d]	7.6	214	8%	2.88 ± 0.09[d]
9 (9, 1)[e]	10	26	1.3%	1.7 ± 0.1[e]
10 (12, 1)[e]	11	15	0.9%	1.40 ± 0.07[e]

[a] n is the number of PEG repeat units; m is the number of PFPE repeat units. [b] Hydrophilic-lipophilic balance (HLB) is calculated using the following equation: HLB= $20*MW_{PEG+amide}/(MW_{Total})$, using the molecular weight (MW) of the PEG segment and amide. [c] Measured in duplicate. [d] Measured by spinning droplet tensiometry by pre-dissolving the fluorosurfactant in HFE-7700. [e] Measured by spinning droplet tensiometry by pre-dissolving the fluorosurfactant in water.

m = 32 and resulted in moderate to low IFT values: **1** (n = 5), 14 ± 0.1 mN m^{-1}; **2** (n = 10), 3.57 ± 0.03 mN m^{-1}; **3** (n = 22), 17.8 ± 0.7 mN m^{-1}, showing a minimum with surfactant **2**. Surfactants **4**–**6** consisted of a PFPE group with m = 9 and also resulted in moderate IFT values: **4** (n = 5), 14.3 ± 0.5 mN m^{-1}; **5** (n = 10), 14.63 ± 0.03 mN m^{-1}; **6** (n = 22), 9 ± 1 mN m^{-1}, showing a minimum with surfactant **6**. Among surfactants **7**–**10** (m = 1), only surfactants **7** and **8** demonstrated appreciable HFE-7700 solubility allowing measurement of IFT by pendant droplet tensiometry; surfactant **7** (n = 3) gave an IFT value of 11.33 ± 0.09 mN m^{-1} and **8** (n = 5) showed the lowest IFT value of all the fluorous soluble surfactants measured, with a value of 2.88 ± 0.07 mN m^{-1}.

All attempts to measure water-soluble fluorosurfactants **9** and **10** *via* the pendant drop tensiometer were inconclusive because their IFT appeared lower than the detection limits of pendant droplet tensiometry (approximately 2 mN m^{-1}). To obtain IFT values for these surfactants we used spinning droplet tensiometry, where a droplet of water in HFE-7700 is inserted within a capillary that spins along the long axis, enabling measurements of low IFT values (Figure S6b). We checked that both techniques provide similar readings of IFT by measuring the IFT of **KP600** using both pendant and spinning droplet tensiometry. Our results for both methods are in agreement with previously reported values for **KP600** (5.4 ± 0.4 mN m^{-1}).[35] We found that both **9** and **10**, when dissolved in the continuous water phase, displayed very low IFTs of 1.7 ± 0.1 mN m^{-1} and 1.40 ± 0.07 mN m^{-1}, respectively. Surfactant **8** was also measured by spinning droplet tensiometry, dissolved in bulk HFE-7700, and an IFT of 2.88 ± 0.09 mN m^{-1} was measured, corroborating the performance of this surfactant.

A common metric employed to predict surface activity of amphiphiles is the hydrophilic lipophilic balance (HLB), herein defined as $20*MW_{PEG+amide}/MW_{Total}$. To evaluate how well IFT–HLB trends hold for the PEG-PFPE surfactants, we plotted the IFT vs.

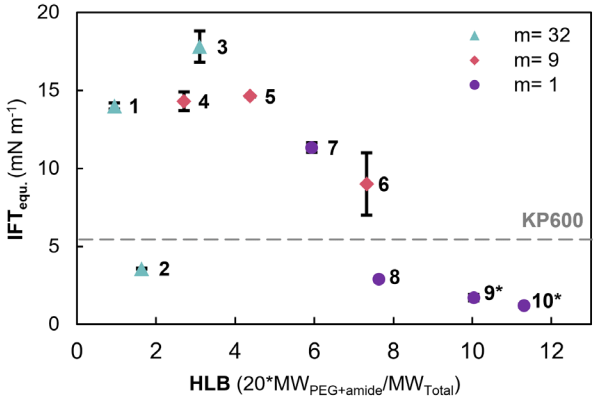

Figure 2. Dependence of minimum IFTs for surfactants **1**–**8** dissolved in HFE-7700 vs. bulk water, determined by the pendant droplet method, and surfactants **9** and **10** dissolved in water vs. bulk HFE-7700, determined by the spinning droplet method, at concentrations above the cmc on the hydrophilic–lipophilic balance (HLB) (see values in Table 1).

HLB for **1**–**10**. (Figure 2). Although there is no clear linear relationship across surfactants **1**–**10**, it can be seen that overall there is decreasing IFT with increasing HLB (*i.e.* proportion of PEG within the surfactant molecule). This trend holds even when the surfactant preferentially partitions into the aqueous phase (surfactants **9, 10**).

Overall, four of the ten custom diblock PEG_nPFPE_m surfactants (**2**, **8**–**10**) displayed an IFT for the perfluorocarbon/water interface lower than that of commercial **KP600** (Figure 2). Surfactant **2** is an outlier in the IFT vs. HLB analysis. We are confident in the measurement of **2** but future investigations are necessary to determine the cause of its outlying nature. Surfactants **8**–**10** are those with the highest HLB ratios, with **9** and **10** being so hydrophilic that they display significant water solubility, which complicates their use in *in vivo* applications. Surfactant **8** provides the lowest IFT values while retaining fluorous solubility. Hence, we selected surfactant **8** as the most promising surfactant of the panel, being able to lower the IFT of the HFE-7700/water interface to nearly half that of **KP600**. We further characterized the ability of surfactant **8** to stabilize biologically relevant interfaces.

Further characterization of low IFT fluorous soluble PEG_5PFPE_1 surfactant

Having identified surfactant **8**, now deemed **PEG_5PFPE_1**, as being able to stabilize perfluorocarbon/water interfaces with a low IFT, we looked to fully understand its behavior before using it *in vivo*. A thorough set of concentration dependent pendant droplet tensiometry measurements indicated that the cmc of **PEG_5PFPE_1** in HFE-7700 was 180 mM (Figure 3a), which corresponds to 6.8 wt% in HFE-7700. This cmc value is quite high, which is consistent with the excellent fluorous solubility observed for **PEG_5PFPE_1** (up to 900 mM, Figure S8).

Next, we analyzed the effect of salt on the IFT. Generally, non-ionic surfactants provide robust interfacial stability[35] when the ionic strength or pH of the continuous phase is altered and only very minor shifts in IFT at high ionic strength conditions are seen when compared to ionic surfactants.[36–38] We measured the IFT of **PEG_5PFPE_1** within increasing ionic strength saline by pendant droplet tensiometry (Figure 3b; Table 2). Upon increasing NaCl concentration from 0 to 100 mM, a negligible decrease in IFT was seen (-0.06 mN m^{-1}). Further increases in NaCl concentrations to 500 and 1000 mM resulted in moderate increases in measured IFT (+0.79 and +0.87 mN m^{-1}, respectively); however, these ion

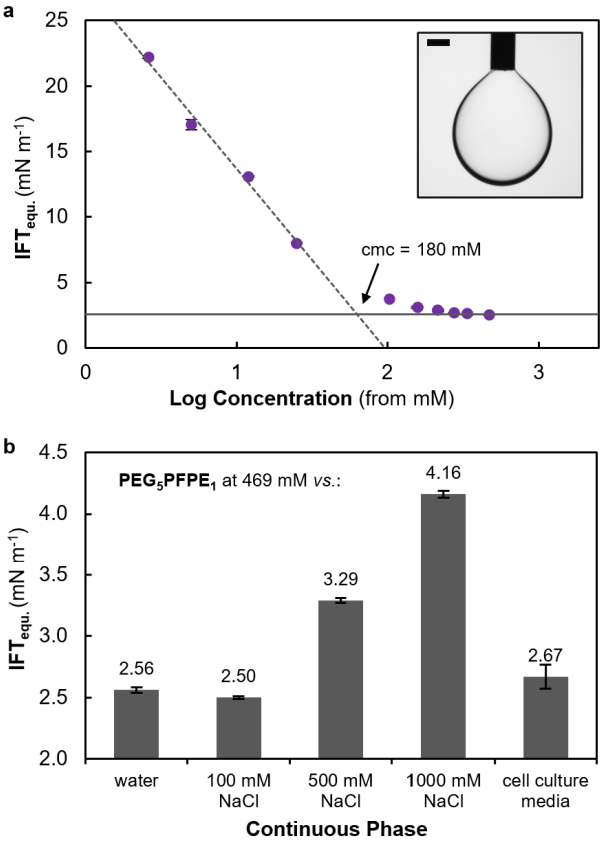

Figure 3. Interfacial tension (IFT) analysis of surfactant by pendant droplet tensiometry of **PEG$_5$PFPE$_1$**. a) Relationship of the log concentration of **PEG$_5$PFPE$_1$** in HFE-7700 with the equilibrium IFT measured by pendant droplet tensiometry in water; a representative droplet is shown in the inset (scale bar= 0.25 mm). b) Measured equilibrium IFT values of **PEG$_5$PFPE$_1$** (469 mM, 16 wt%) vs. bulk aqueous solutions of various ionic strengths: water, NaCl solutions (100, 500, and 1000 mM), and cell culture media (RPMI, 10 vol% fetal bovine serum, and 1 *w/v*% penicillin/streptomycin).

concentrations are above those commonly encountered in biological systems: zebrafish embryos and mammalian cell culture have typical equivalent ion concentrations between 105–193 mM.[1]

To further mimic a living system, we performed IFT measurements of **PEG$_5$PFPE$_1$** in HFE-7700 vs. mammalian cell culture media (RPMI) containing 10 *vol*% fetal bovine serum and 1 *w/v*% penicillin/streptomycin antibiotic. A minimal increase in IFT was seen with bulk cell culture media (+0.11 mN m^{-1}), corroborating the NaCl results and suggesting minimal interactions with proteins. Although only **PEG$_5$PFPE$_1$** was tested in cell culture media, we anticipate that all diblock PEG$_n$PFPE$_m$ surfactants show robust interfacial stabilization in moderate ionic strength conditions owning to their non-ionic character. Overall, these data suggest that **PEG$_5$PFPE$_1$** is well-suited for biological applications. We therefore proceeded to test its performance in direct *in vivo* measurements of mechanical stresses within developing zebrafish embryos.

Applications of PEG$_5$PFPE$_1$ to in vivo *force measurements*

Over the past decade, Campàs and coworkers have developed technologies to measure intercellular forces,[31,32] tissue material properties,[33,34] and osmotic pressures[1] *in situ* and *in vivo*. These technologies involve fluorescence imaging of perfluorocarbon microdroplets previously inserted into tissue.[31–33,39] In the case of force (or mechanical stress) measurements, cell-sized PFC microdroplets are inserted into living tissues and, if the IFT is low enough, the cellular and tissue forces deform the droplet.[31] The

Table 2. Measured IFTs of **PEG$_5$PFPE$_1$** (469 mM, 16 wt%) using pendant droplet tensiometry against bulk aqueous solutions of various ionic strengths. Values reported are the average measured value of three droplets and the standard deviation.

Ionic Solute	Ion Concentration (mM)	IFT$_{equ.}$ (mN m^{-1})
none	0	2.56 ± 0.02
NaCl	100	2.50 ± 0.01
NaCl	500	3.29 ± 0.02
NaCl	1000	4.16 ± 0.03
Cell culture media[a]	169	2.7 ± 0.1

[a] Mammalian cell culture media formulated with RPMI (inorganic salts, vitamins, *etc.*), 10 vol% fetal bovine serum (FBS), and 1 *w/v*% penicillin/streptomycin.

shape of the droplet is reconstituted in 3D using confocal microscopy, and the endogenous stresses are then quantified from the deformations of the droplet and knowledge of the droplet IFT.[31,40,41] If the IFT is too large, cells cannot deform the droplet, precluding any measurements. Therefore, lower IFT values enhance the measurement sensitivity (better signal-to-noise) as they allow cells to deform the droplets more easily. To date these technologies have relied on commercially available **KP600** to lower the IFT of the PFC droplet,[35,42] such that intercellular forces can deform the droplet. While mechanical measurements were possible in mouse tissues,[42] albeit with limited sensitivity, force measurements in zebrafish tissues or in many other systems were not possible because cells in these other organisms feature smaller forces. **PEG$_5$PFPE$_1$**, with an IFT approximately half that of **KP600**, appeared primed to expand the capabilities of *in vivo* force measurements to a wide range of organisms.

To demonstrate the potential of **PEG$_5$PFPE$_1$**, we aimed to measure forces in the presomitic mesoderm of developing zebrafish embryos, which are below the limit of detection with **KP600**. We first characterized the IFT of **PEG$_5$PFPE$_1$** in the presence of the fluorophores (**FCy5**[43]**,** Figure S1), zebrafish embryo media (E3), and potential co-surfactants (**KP600**) using the spinning drop tensiometer benchmarked to **KP600** (Figure 4). Previously **KP600** (2 wt%) was used to lower the IFT of HFE-7700 vs. water (5.4 ± 0.4 mN m^{-1}). **PEG$_5$PFPE$_1$** (8 wt%, 3.01 mN m^{-1}) alone decreases the IFT with water to about half (45% reduction) that of **KP600** (2 wt%), similar to findings from pendant droplet tensiometry measurements. Inclusion of **FCy5** with **PEG$_5$PFPE$_1$** leads to only a minor increase in IFT vs. **PEG$_5$PFPE$_1$** alone (3.17 mN m^{-1},

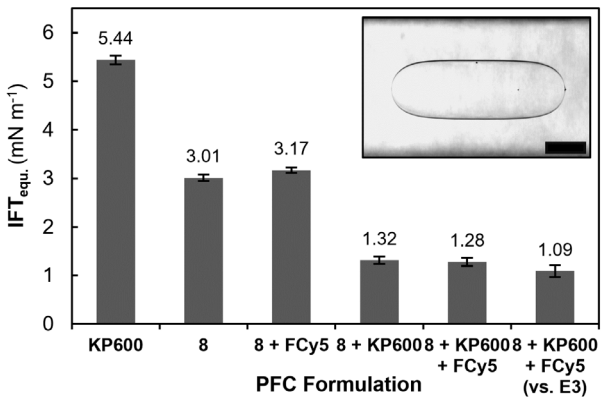

Figure 4. Formulation analysis of **PEG$_5$PFPE$_1$** (**8**), commercial **KP600**, and fluorescent dye **FCy5**. Measured vs. water unless otherwise specified using spinning droplet tensiometry. A representative droplet is shown in the inset (scale bar= 1 mm).

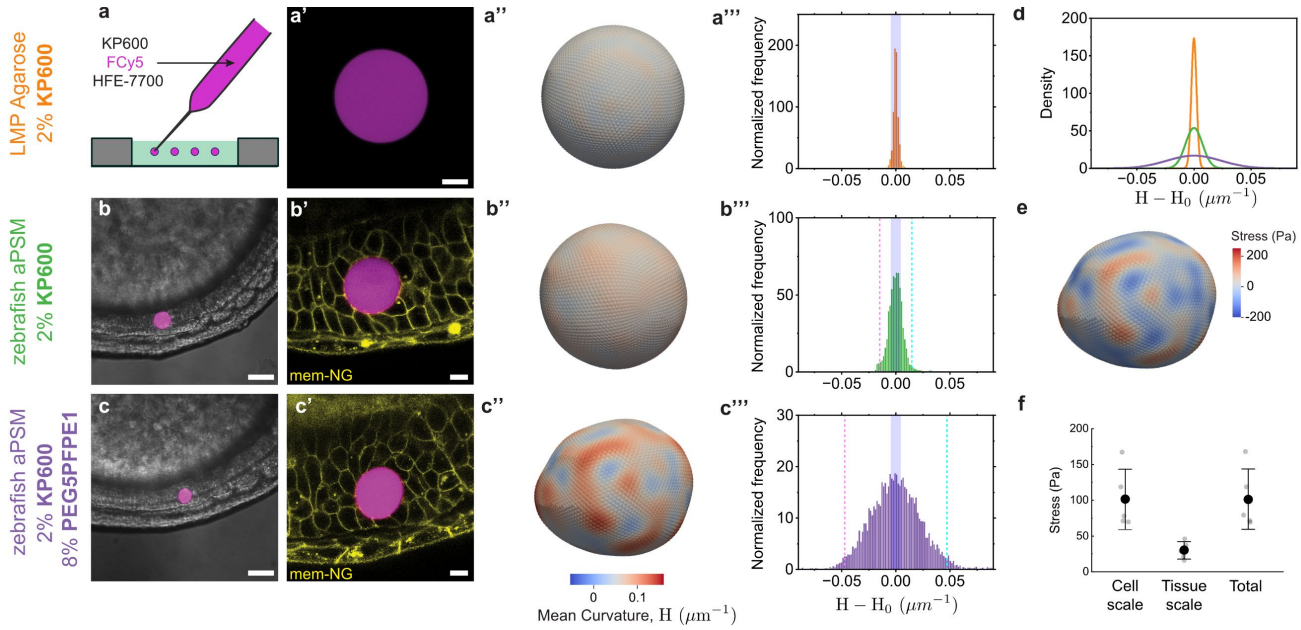

Figure 5. Comparison of droplet deformations with different surfactants. (a-a''') Spherical droplets (HFE-7700 with **KP600** at 2 wt% and **FCy5**) are inserted into warm (fluid) low MP agarose (a) and imaged under confocal microscopy after the agarose jellified (a'). Droplets are reconstructed in 3D, the mean curvature H is obtained at every point of the surface (a''), and the normalized frequency of H-H_0 (H_0 being the average mean curvature) is obtained (a'''). The purple shaded region in the histogram denotes the 95th percentile of the H-H_0 distribution, which provides a quantitative estimate of the deformation detection threshold. (b-c''') Confocal sections of droplets containing **KP600** (2 wt%) and **FCy5** (b-b') or **KP600** (2 wt%), **PEG_5PFPE_1** (8 wt%) and **FCy5** (c,c') inserted in the anterior presomitic mesoderm (aPSM) region of zebrafish embryos at approximately 10 somite stage (b', c'; **FCy5**, magenta; cell membranes, yellow). Droplets are reconstructed in 3D, the mean curvature H is obtained at every point of the surface is obtained (b'', c''), and the normalized frequency distribution of H-H_0 are obtained (b''', c''') in each case. Light blue and pink dashed lines indicate two standard deviations. The purple shaded region in the histogram denotes the detection threshold obtained in a'''. (d) Comparison of the density distributions for each condition (orange: **KP600** (2 wt%) in LMP agarose; green: **KP600** in zebrafish aPSM; purple: **KP600+PEG_5PFPE_1** in zebrafish aPSM). (e) Mechanical stresses at each point on the droplet surface for a representative droplet containing the novel **KP600+PEG_5PFPE_1** in the aPSM of a developing zebrafish embryo at the 10-somite stage. (f) Measured total mechanical stresses, as well as stresses at cell- and tissue-scales in the aPSM of zebrafish embryos (n=5), obtained from droplets with the novel **KP600+PEG_5PFPE_1** system. Scale bars, black = 50 μm; white= 10 μm.

+2%). We note that we have previously observed **FCy5** to associate at perfluorocarbon/water interfaces and thus it may possess some surfactant-like properties; however these appear minimal compared to the efficacy of **PEG_5PFPE_1**.

Since **KP600** and **PEG_5PFPE_1** feature different physical sizes, we envisioned that their combination may lead to a better surface packing of the surfactants and a further reduction in IFT. A mixed surfactant system consisting of **KP600** (2 wt%) and **PEG_5PFPE_1** (8 wt%) indeed results in an even lower IFT of 1.32 mN m^{-1}, a ~75% reduction from **KP600** alone. Introduction of **FCy5** to the **KP600+PEG_5PFPE_1** surfactant system retained a low IFT (1.28 mN m^{-1}) in water. Finally, we measured the complete system in E3 embryo media used for zebrafish embryo development and determined a remarkably low IFT of 1.09 mN m^{-1} for the full system. We find a reduction of approximately 5-fold compared to using **KP600** alone, which should translate to a substantial increase in the sensitivity of mechanical stress measurements.

To quantify the ability of **PEG_5PFPE_1** to improve microdroplet mechanical force sensing *in vivo*, we first characterized the sensitivity threshold of oil droplets by embedding spherical PFC droplets (**KP600** (2 wt%) and **FCy5** (100 μM) in HFE-7700) in low-meting point agarose (1 *w/v*%; Figure 5a). In this system, any deviations from the spherical state are noise, as the gel-confined, spherical microdroplet experiences no net forces. We imaged the spherical droplets in 3D using confocal microscopy (Figure 5a') and reconstructed the surface deformations using previously developed STRESS software[41] (Figure 5a''). The width of the distribution of surface mean curvature, H, quantifies the deviations of the droplet curvature from the expected constant mean curvature, H_0, of the spherical droplet. Therefore, H–H_0 provides direct quantification of the curvature measurement noise, defining the detection threshold for droplet deformations at absolute values of mean curvatures above 0.0046 μm^{-1} (Figure 5a'''). Measured relative errors of the mean curvature were below 10%, as previously established.[40]

Having determined our measurement sensitivity, we inserted the fluorous formulation (**KP600** (2 wt%) and **FCy5** (100 μM) in HFE-7700) without and with **PEG_5PFPE_1** (8 wt%) into the anterior presomitic mesoderm (aPSM) of developing zebrafish embryos. Inserted microdroplets, without (Figure b-b''') and with **PEG_5PFPE_1** (Figure c-c'''), were imaged using confocal microscopy (Figure 5b, b' and c, c'), 3D reconstructed and the distribution of droplet mean curvature, H, was quantified using the STRESS software[41] (Figure 5 b'', c''). We then obtained the normalized frequency distribution of the deviations of the mean curvature H from the average mean curvature H_0 in each condition (Figure 5b''', c'''). Our measurements indicate that PFC microdroplets containing **KP600** alone deform less (Figure 5b''') than droplets containing both **KP600** and **PEG_5PFPE_1** (Figure 5c'''), as shown by the considerably wider mean curvature distribution with **PEG_5PFPE_1** (Figure 5c'''). For droplets containing only **KP600** in the embryos, we see that the curvature distribution (Figure 5b''') is very close to the detection limit quantified with spherical droplets (Figure 5a'''), indicating that measurements of mechanical stresses with **KP600** are close to noise levels. Gaussian fits of each distribution are shown in Figure 5d, allowing their comparison.

To avoid errors associated with outliers, we obtained the largest and smallest curvature values after removing the top and bottom 2.5% of the curvature distribution (demarcated by the pink and blue vertical dashed lines in Figure 5b''', c'''). The measured maximal and minimal values of H–H_0 for droplets with only **KP600** are ±0.0148 μm^{-1}, which correspond to a relative difference factor from the detection threshold of 2.2, indicating that the measured deformations are relatively close to the detection threshold, highlighting the low signal-to-noise ratio in measurements with only

KP600. Droplets with both **KP600** and **PEG_5PFPE_1** display maximal and minimal values of $H–H_0$ of $\pm 0.047\ \mu m^{-1}$, corresponding to a relative difference factor from the detection threshold of 9.2, indicating a much larger signal-to-noise (nearly a factor of 10). Droplets with **PEG_5PFPE_1** and **KP600** feature signal levels 4.2 times larger than droplets without **PEG_5PFPE_1**, a factor similar to the relative change in IFT in the two conditions (a factor of 4).

Using the measured IFT value of droplets with **KP600** and **PEG_5PFPE_1** in E3 media, we quantified the anisotropic stresses in the aPSM of living zebrafish embryos, both for a single droplet (3D stress map; Figure 5e) and also the stress measurement statistics for multiple droplets (Figure 5f). The measured values of both the cellular-scale stresses (deviations from the ellipsoidal mode) and tissue-scale stresses (ellipsoidal deformations) are comparable to those previously quantified with magnetic microdroplets within same tissues;[33] however, this novel system is drastically less experimentally demanding and does not require magnetic actuation. The measured values of stresses obtained herein display substantially reduced dispersion compared to measurements with magnetic microdroplets, which we attribute to the well-defined, low IFT of non-ionic **PEG_5PFPE_1** droplets compared to magnetic droplets that contain poorly characterized ionic surfactants. Our results show that **PEG_5PFPE_1** enables robust mechanical measurements of cell and tissue stresses with unprecedented resolution and simplicity.

Conclusions

The synthesis of novel non-ionic fluorosurfactants covering a wide molecular weight range (MW= 0.64–66 kDa) and mass balance of the hydrophilic and fluorophilic segments (HLB= 0.95–11) has allowed us to identify surfactants that give low IFT values and high PFC solubility, requisite for sensitive mechanical measurements with fluorocarbon oil microdroplets. **PEG_5PFPE_1** (MW= 0.73 kDa, HLB= 7.6) was identified as the premier surfactant demonstrating a low minimum IFT (2.63 ± 0.08 mM m^{-1}) combined with high PFC solubilities (cmc= 180 mM in HFE-7700). Synergistically, the combination of commercially available **KP600** with **PEG_5PFPE_1** allowed for an approximately five-fold reduction in the IFT of formulations of PFC force sensing microdroplets. This drastic decrease allows for sensitive measurements of mechanical stresses in developing embryonic tissues in a manner that is more facile, more stable, and more sensitive than previous methods containing fluorous ferrofluids with ionic surfactants. This increased sensitivity afforded by addition of **PEG_5PFPE_1** is anticipated to allow for measurements of intercellular and tissue level forces in a wider array of samples, including embryos from different species and a wide range of organoids.

Although optimized for perfluorocarbon-in-water microdroplets, fluorous surfactants described herein may be of utility in applications beyond that of *in vivo* force sensing. For example, enabling functionality in ultrasonic manipulation[27–30] of perfluorocarbon emulsions. **PEG_5PFPE_1** may also find utility in microfluidic systems comprised of water-in-perfluorocarbon microdroplets as a synthetically accessible and purifiable component that can be produced at scale.[3] **PEG_5PFPE_1** can be adopted into multi-component and complex nanoemulsions as an additional tool to stabilize increasingly complex architectures, whereas high solubilities of **PEG_5PFPE_1** in perfluorocarbons can ostensibly reduce the fraction of perfluorocarbon solvent and phase densities. Beyond biomedical applications, fluorosurfactants have also found utility in greener syntheses with supercritical CO_2 ($scCO_2$) as an efficient surfactant that can be recycled from products by chromatography.[44–46] With exceptional IFT lowering capabilities, high perfluorocarbon solubility, facile synthesis and purification, **PEG_5PFPE_1**, composed with a short perfluoropolyether fluorous segment, is privileged to control the interface of fluorocarbons in a variety of complex environments, including tissues.

Supporting Information

Supporting Information containing supplementary figures, materials and methods, experimental procedures, and spectroscopic information is available. The authors have cited additional references in the Supporting Information. [4,41,43,47–49]

Acknowledgements

We would like to acknowledge Dr. Carlos Gomez for fruitful discussion and performing preliminary *in situ* experiments, Dr. Irene Lim for synthesis of fluorous soluble cyanine dyes used to visualize droplets, Claudia Fröb for discussions and inputs on the interfacial tension experiments, and the animal resource center of UC Santa Barbara for the zebrafish colony husbandry work. M.V. was supported by the Human Frontier Science Program (HFSP) fellowship LT000283-2020-C. J.G. was supported by a Cota Robles Fellowship. This work was supported by NIGMS (R01GM135380 to O.C. and E.M.S.) and by the Deutsche Forschungsgemeinschaft (DFG, German Research Foundation) under Germany's Excellence Strategy – EXC 2068 – 390729961– Cluster of Excellence Physics of Life of TU Dresden.

Keywords: surfactant • fluorosurfactant • perfluoropolyether • *in vivo* force sensing • microdroplets

References

(1) Vian, A.; Pochitaloff, M.; Yen, S. T.; Kim, S.; Pollock, J.; Liu, Y.; Sletten, E. M.; Campàs, O. In Situ Quantification of Osmotic Pressure within Living Embryonic Tissues. *Nat. Commun.* **2023**, *14* (1), 1–10. https://doi.org/10.1038/s41467-023-42024-9.

(2) Krafft, M. P. Fluorocarbons and Fluorinated Amphiphiles in Drug Delivery and Biomedical Research. *Adv. Drug Deliv. Rev.* **2001**, *47* (2–3), 209–228. https://doi.org/10.1016/S0169-409X(01)00107-7.

(3) Battat, S.; Weitz, D. A.; Whitesides, G. M. An Outlook on Microfluidics: The Promise and the Challenge. *Lab Chip* **2022**, *22* (3), 530–536. https://doi.org/10.1039/D1LC00731A.

(4) Holtze, C.; Rowat, A. C.; Agresti, J. J.; Hutchison, J. B.; Angilè, F. E.; Schmitz, C. H. J.; Köster, S.; Duan, H.; Humphry, K. J.; Scanga, R. A.; Johnson, J. S.; Pisignano, D.; Weitz, D. A. Biocompatible Surfactants for Water-in-Fluorocarbon Emulsions. *Lab Chip* **2008**, *8* (10), 1632–1639. https://doi.org/10.1039/b806706f.

(5) Baret, J. C. Surfactants in Droplet-Based Microfluidics. *Lab Chip* **2012**, *12* (3), 422–433. https://doi.org/10.1039/C1LC20582J.

(6) Holt, D. J.; Payne, R. J.; Chow, W. Y.; Abell, C. Fluorosurfactants for Microdroplets: Interfacial Tension Analysis. *J. Colloid Interface Sci.* **2010**, *350* (1), 205–211. https://doi.org/10.1016/j.jcis.2010.06.036.

(7) Rosen, M. J.; Kunjappu, J. T. Surfactants and Interfacial Phenomena: Fourth Edition. *Surfactants Interfacial Phenom. Fourth Ed.* **2012**. https://doi.org/10.1002/9781118228920.

(8) Puts, G. J.; Crouse, P.; Ameduri, B. M. Polytetrafluoroethylene: Synthesis and Characterization of the Original Extreme Polymer. *Chem. Rev.* **2019**, *119* (3), 1763–1805. https://doi.org/10.1021/acs.chemrev.8b00458.

(9) Chiu, Y. L.; Chan, H. F.; Phua, K. K. L.; Zhang, Y.; Juul, S.; Knudsen, B. R.; Ho, Y. P.; Leong, K. W. Synthesis of Fluorosurfactants for Emulsion-Based Biological

Applications. *ACS Nano* **2014**, *8* (4), 3913–3920. https://doi.org/10.1021/NN500810N/SUPPL_FILE/NN500810N_SI_001.PDF.

(10) Wagner, O.; Thiele, J.; Weinhart, M.; Mazutis, L.; Weitz, D. A.; Huck, W. T. S.; Haag, R. Biocompatible Fluorinated Polyglycerols for Droplet Microfluidics as an Alternative to PEG-Based Copolymer Surfactants. *Lab Chip* **2016**, *16* (1), 65–69. https://doi.org/10.1039/C5LC00823A.

(11) Scanga, R.; Chrastecka, L.; Mohammad, R.; Meadows, A.; Quan, P. L.; Brouzes, E. Click Chemistry Approaches to Expand the Repertoire of PEG-Based Fluorinated Surfactants for Droplet Microfluidics. *RSC Adv.* **2018**, *8* (23), 12960–12974. https://doi.org/10.1039/c8ra01254g.

(12) Chowdhury, M. S.; Zheng, W.; Kumari, S.; Heyman, J.; Zhang, X.; Dey, P.; Weitz, D. A.; Haag, R. Dendronized Fluorosurfactant for Highly Stable Water-in-Fluorinated Oil Emulsions with Minimal Inter-Droplet Transfer of Small Molecules. *Nat. Commun. 2019 101* **2019**, *10* (1), 1–10. https://doi.org/10.1038/s41467-019-12462-5.

(13) Chowdhury, M. S.; Zheng, W.; Singh, A. K.; Ong, I. L. H.; Hou, Y.; Heyman, J. A.; Faghani, A.; Amstad, E.; Weitz, D. A.; Haag, R. Linear Triglycerol-Based Fluorosurfactants Show High Potential for Droplet-Microfluidics-Based Biochemical Assays. *Soft Matter* **2021**, *17* (31), 7260–7267. https://doi.org/10.1039/D1SM00890K.

(14) Kunieda, H.; Shinoda, K. Krafft Points, Critical Micelle Concentrations, Surface Tension, and Solubilizing Power of Aqueous Solutions of Fluorinated Surfactants. *J. Phys. Chem.* **1976**, *80* (22), 2468–2470. https://doi.org/10.1021/J100563A007/ASSET/J100563A007.FP.PNG_V03.

(15) Zaggia, A.; Ameduri, B. Recent Advances on Synthesis of Potentially Non-Bioaccumulable Fluorinated Surfactants. *Curr. Opin. Colloid Interface Sci.* **2012**, *17* (4), 188–195. https://doi.org/10.1016/J.COCIS.2012.04.001.

(16) Zhou, R.; Jin, Y.; Shen, Y.; Zhao, P.; Zhou, Y. Synthesis and Application of Non-Bioaccumulable Fluorinated Surfactants: A Review. *J. Leather Sci. Eng.* **2021**, *3* (1), 1–15. https://doi.org/10.1186/S42825-020-00048-7/FIGURES/6.

(17) O'Neal, K. L.; Geib, S.; Weber, S. G. Extraction of Pyridines into Fluorous Solvents Based on Hydrogen Bond Complex Formation with Carboxylic Acid Receptors. *Anal. Chem.* **2007**, *79* (8), 3117–3125. https://doi.org/10.1021/ac062287+.

(18) Klein, A. M.; Mazutis, L.; Akartuna, I.; Tallapragada, N.; Veres, A.; Li, V.; Peshkin, L.; Weitz, D. A.; Kirschner, M. W. Droplet Barcoding for Single-Cell Transcriptomics Applied to Embryonic Stem Cells. *Cell* **2015**, *161* (5), 1187–1201. https://doi.org/10.1016/J.CELL.2015.04.044.

(19) Zheng, W.; Zhao, S.; Yin, Y.; Zhang, H.; Needham, D. M.; Evans, E. D.; Dai, C. L.; Lu, P. J.; Alm, E. J.; Weitz, D. A. High-Throughput, Single-Microbe Genomics with Strain Resolution, Applied to a Human Gut Microbiome. *Science (80-.).* **2022**, *376* (6597), eabm1483. https://doi.org/10.1126/science.abm1483.

(20) Li, X.; Tang, S. Y.; Zhang, Y.; Zhu, J.; Forgham, H.; Zhao, C. X.; Zhang, C.; Davis, T. P.; Qiao, R. Tailored Fluorosurfactants through Controlled/Living Radical Polymerization for Highly Stable Microfluidic Droplet Generation. *Angew. Chemie - Int. Ed.* **2024**, *63* (3). https://doi.org/10.1002/anie.202315552.

(21) Junge, F.; Lee, P. W.; Kumar Singh, A.; Wasternack, J.; Pachnicz, M. P.; Haag, R.; Schalley, C. A. Interfaces with Fluorinated Amphiphiles: Superstructures and Microfluidics. *Angew. Chemie Int. Ed.* **2023**, *62* (12), e202213866. https://doi.org/10.1002/ANIE.202213866.

(22) Krafft, M. P.; Riess, J. G. Therapeutic Oxygen Delivery by Perfluorocarbon-Based Colloids. *Adv. Colloid Interface Sci.* **2021**, *294*, 102407. https://doi.org/10.1016/J.CIS.2021.102407.

(23) Abdalkader, R.; Kawakami, S.; Unga, J.; Higuchi, Y.; Suzuki, R.; Maruyama, K.; Yamashita, F.; Hashida, M. The Development of Mechanically Formed Stable Nanobubbles Intended for Sonoporation-Mediated Gene Transfection. *Drug Deliv.* **2017**, *24* (1), 320–327. https://doi.org/10.1080/10717544.2016.1250139.

(24) Estabrook, D. A.; Day, R. A.; Sletten, E. M. Redox-Responsive Gene Delivery from Perfluorocarbon Nanoemulsions through Cleavable Poly(2-Oxazoline) Surfactants. *Angew. Chemie Int. Ed.* **2021**, *60* (32), 17362–17367. https://doi.org/10.1002/ANIE.202102413.

(25) Estabrook, D. A.; Chapman, J. O.; Yen, S. T.; Lin, H. H.; Ng, E. T.; Zhu, L.; van de Wouw, H. L.; Campàs, O.; Sletten, E. M. Macromolecular Crowding as an Intracellular Stimulus for Responsive Nanomaterials. *J. Am. Chem. Soc.* **2022**, *144* (37), 16792–16798. https://doi.org/10.1021/JACS.2C03064/ASSET/IMAGES/LARGE/JA2C03064_0007.JPEG.

(26) Day, R. A.; Estabrook, D. A.; Logan, J. K.; Sletten, E. M. Fluorous Photosensitizers Enhance Photodynamic Therapy with Perfluorocarbon Nanoemulsions. *Chem. Commun.* **2017**, *53* (97), 13043–13046. https://doi.org/10.1039/C7CC07038A.

(27) Tran, T. D.; Caruthers, S. D.; Hughes, M.; Marsh, J. N.; Cyrus, T.; Winter, P. M.; Neubauer, A. M.; Wickline, S. A.; Lanza, G. M. Clinical Applications of Perfluorocarbon Nanoparticles for Molecular Imaging and Targeted Therapeutics. *Int. J. Nanomedicine* **2007**, *2* (4), 515–526.

(28) Sheeran, P. S.; Dayton, P. A. Improving the Performance of Phase-Change Perfluorocarbon Droplets for Medical Ultrasonography: Current Progress, Challenges, and Prospects. *Scientifica (Cairo).* **2014**, *2014*, 1–24. https://doi.org/10.1155/2014/579684.

(29) Huang, Y.; Vezeridis, A. M.; Wang, J.; Wang, Z.; Thompson, M.; Mattrey, R. F.; Gianneschi, N. C. Polymer-Stabilized Perfluorobutane Nanodroplets for Ultrasound Imaging Agents. *J. Am. Chem. Soc.* **2017**, *139* (1), 15–18. https://doi.org/10.1021/jacs.6b08800.

(30) Rapoport, N.; Nam, K.-H. H.; Gupta, R.; Gao, Z.; Mohan, P.; Payne, A.; Todd, N.; Liu, X.; Kim, T.; Shea, J.; Scaife, C.; Parker, D. L.; Jeong, E.-K. K.; Kennedy, A. M. Ultrasound-Mediated Tumor Imaging and Nanotherapy Using Drug Loaded, Block Copolymer Stabilized Perfluorocarbon Nanoemulsions. *J. Control. Release* **2011**, *153* (1), 4–15. https://doi.org/10.1016/J.JCONREL.2011.01.022.

(31) Campàs, O.; Mammoto, T.; Hasso, S.; Sperling, R. A.; O'connell, D.; Bischof, A. G.; Maas, R.; Weitz, D. A.; Mahadevan, L.; Ingber, D. E. Quantifying Cell-Generated Mechanical Forces within Living Embryonic Tissues. *Nat. Methods* **2014**, *11* (2), 183–189. https://doi.org/10.1038/nmeth.2761.

(32) Mongera, A.; Rowghanian, P.; Gustafson, H. J.; Shelton, E.; Kealhofer, D. A.; Carn, E. K.; Serwane, F.; Lucio, A. A.; Giammona, J.; Campàs, O. A Fluid-to-Solid Jamming Transition Underlies Vertebrate Body Axis Elongation. *Nature* **2018**, *561* (7723), 401–405. https://doi.org/10.1038/s41586-018-0479-2.

(33) Serwane, F.; Mongera, A.; Rowghanian, P.; Kealhofer, D. A.; Lucio, A. A.; Hockenbery, Z. M.; Campàs, O. In Vivo Quantification of Spatially Varying Mechanical Properties in Developing Tissues. *Nat. Methods* **2017**, *14* (2), 181–186. https://doi.org/10.1038/nmeth.4101.

(34) Mongera, A.; Pochitaloff, M.; Gustafson, H. J.; Stooke-

Vaughan, G. A.; Rowghanian, P.; Kim, S.; Campàs, O. Mechanics of the Cellular Microenvironment as Probed by Cells in Vivo during Zebrafish Presomitic Mesoderm Differentiation. *Nat. Mater. 2022 221* **2023**, *22* (1), 135–143. https://doi.org/10.1038/s41563-022-01433-9.

(35) Lucio, A. A.; Mongera, A.; Shelton, E.; Chen, R.; Doyle, A. M.; Campàs, O. Spatiotemporal Variation of Endogenous Cell-Generated Stresses within 3D Multicellular Spheroids. *Sci. Reports 2017 71* **2017**, *7* (1), 1–11. https://doi.org/10.1038/s41598-017-12363-x.

(36) Schott, H. Salting in of Nonionic Surfactants by Complexation with Inorganic Salts. *J. Colloid Interface Sci.* **1973**, *43* (1), 150–155. https://doi.org/10.1016/0021-9797(73)90358-5.

(37) Santos, F. K. G.; Neto, E. L. B.; Moura, M. C. P. A.; Dantas, T. N. C.; Neto, A. A. D. Molecular Behavior of Ionic and Nonionic Surfactants in Saline Medium. *Colloids Surfaces A Physicochem. Eng. Asp.* **2009**, *333* (1–3), 156–162. https://doi.org/10.1016/J.COLSURFA.2008.09.040.

(38) Akhlaghi, N.; Riahi, S.; Parvaneh, R. Interfacial Tension Behavior of a Nonionic Surfactant in Oil/Water System; Salinity, PH, Temperature, and Ionic Strength Effects. *J. Pet. Sci. Eng.* **2021**, *198*, 108177. https://doi.org/10.1016/J.PETROL.2020.108177.

(39) Kim, S.; Pochitaloff, M.; Stooke-Vaughan, G. A.; Campàs, O. Embryonic Tissues as Active Foams. *Nat. Phys. 2021 177* **2021**, *17* (7), 859–866. https://doi.org/10.1038/s41567-021-01215-1.

(40) Shelton, E.; Serwane, F.; Campàs, O. Geometrical Characterization of Fluorescently Labelled Surfaces from Noisy 3D Microscopy Data. *J. Microsc.* **2018**, *269* (3), 259–268. https://doi.org/10.1111/jmi.12624.

(41) Gross, B.; Shelton, E.; Gomez, C.; Campàs, O. STRESS, an Automated Geometrical Characterization of Deformable Particles for in Vivo Measurements of Cell and Tissue Mechanical Stresses. *bioRxiv* **2021**, 2021.03.26.437148. https://doi.org/10.1101/2021.03.26.437148.

(42) Parada, C.; Banavar, S. P.; Khalilian, P.; Rigaud, S.; Michaut, A.; Liu, Y.; Joshy, D. M.; Campàs, O.; Gros, J. Mechanical Feedback Defines Organizing Centers to Drive Digit Emergence. *Dev. Cell* **2022**, *57* (7), 854-866.e6. https://doi.org/10.1016/j.devcel.2022.03.004.

(43) Lim, I.; Vian, A.; van de Wouw, H. L.; Day, R. A.; Gomez, C.; Liu, Y.; Rheingold, A. L.; Campàs, O.; Sletten, E. M. Fluorous Soluble Cyanine Dyes for Visualizing Perfluorocarbons in Living Systems. *J. Am. Chem. Soc.* **2020**, *142* (37), 16072–16081. https://doi.org/10.1021/jacs.0c07761.

(44) Hessel, V.; Tran, N. N.; Asrami, M. R.; Tran, Q. D.; Van Duc Long, N.; Escribà-Gelonch, M.; Tejada, J. O.; Linke, S.; Sundmacher, K. Sustainability of Green Solvents-Review and Perspective. *Green Chemistry*. Royal Society of Chemistry 2022, pp 410–437. https://doi.org/10.1039/d1gc03662a.

(45) Sagisaka, M.; Iwama, S.; Yoshizawa, A.; Mohamed, A.; Cummings, S.; Eastoe, J. Effective and Efficient Surfactant for CO2 Having Only Short Fluorocarbon Chains. *Langmuir* **2012**, *28* (30), 10988–10996. https://doi.org/10.1021/LA301305Q.

(46) Ren, H. R.; Xu, Q. Q.; Yin, J. Z. Microscopic Properties and Stabilization Mechanism of a Supercritical Carbon Dioxide Microemulsion with Extremely High Water Content. *J. Colloid Interface Sci.* **2022**, *607*, 1953–1962. https://doi.org/10.1016/J.JCIS.2021.09.188.

(47) Viades-Trejo, J.; Gracia-Fadrique, J. Spinning Drop Method: From Young–Laplace to Vonnegut. *Colloids Surfaces A Physicochem. Eng. Asp.* **2007**, *302* (1–3), 549–552. https://doi.org/10.1016/J.COLSURFA.2007.03.033.

(48) Schindelin, J.; Arganda-Carreras, I.; Frise, E.; Kaynig, V.; Longair, M.; Pietzsch, T.; Preibisch, S.; Rueden, C.; Saalfeld, S.; Schmid, B.; Tinevez, J. Y.; White, D. J.; Hartenstein, V.; Eliceiri, K.; Tomancak, P.; Cardona, A. Fiji: An Open-Source Platform for Biological-Image Analysis. *Nature Methods*. Nature Publishing Group July 2012, pp 676–682. https://doi.org/10.1038/nmeth.2019.

(49) Nüsslein-Volhard, C.; Dahm, R. *Zebrafish: A Practical Approach*, 1st ed.; Nüsslein-Volhard, C., Dahm, R., Eds.; Oxford University Press: New York, 2002.